Directed evolution of the FdeR allosteric transcription factor and a riboswitch to construct a liquiritigenin biosensor toolkit

Tianqi He[1], Maolong Zhu[1], Yi Liu[1], Yuxin Yang[1], Yuxiang Li[1], Hanzhang Song[1], Yuhao Zhang[1], Jun Liu[1], Xiaohan Ning[1], Yue Zhang[1], Jiaji Lv[1], Yiheng Yang[1], Xi Chen[2*] & Xin Yan[3*]

Abstract

Liquiritigenin, a dihydroflavonoid produced by secondary plant metabolism, has broad applications in food and pharmaceutical industries. However, the production of liquiritigenin still relies on low-yield plant extraction and chemical synthesis currently. Here, we developed biosensors that could identify liquiritigenin specifically based on allosteric transcription factors and riboswitches, enabling the evolution of biomolecules with highly specific new activities. In our future work, we aspire to demonstrate the potential of directed evolution in optimizing biosensors. We are committed to applying the evolved biosensors to intracellular detection of liquiritigenin synthesis and screening of liquiritigenin high yielding strains, thus providing a solution for high-yielding biosynthesis of liquiritigenin.

Key words: liquiritigenin, allosteric transcriptional factor, riboswitch, molecular dynamics simulation, PACE

Introduction

Licorice, is an herbal plant renowned for its distinct sweet flavor. It is called "GAN CAO" in Chinese and is derived from the root or stem of *Glycyrrhiza glabra* (*G. glabra*). Its primary active components consist of triterpenes and flavonoids.

Liquiritigenin is a dihydroxyflavone, one of the main bioactive components extracted from licorice. Its various high-value pharmacological activities have been extensively studied, such as antioxidant, anti-inflammatory, anti-cancer, hepatoprotective, and neuroprotective properties. Furthermore, it also serves as an intermediate for the synthesis of drugs with anti-diabetic, anti-tuberculosis and other properties, offering significant potential and vast application prospects in the healthcare field.[1] The prevalent methods of liquiritigenin production, such as plant extraction and chemical synthesis, have their inherent limitations. The former is constrained by long growth cycles, high costs, and low yields (approximately 1 gram

from 250-33,000 g of dry leguminous plants). The latter involves toxic solvents, extreme reaction conditions, and complex molecular modifications, making it unsuitable for industrial production and harmful to the environment. Microbial production is an attractive candidate for flavonoid production with advantages like low energy consumption, minimal waste, environmental friendliness.[2,3] Although significant research has explored the heterologous synthesis of 5-deoxy(iso)flavonoids in microbial hosts, the yield remains relatively low.[4,5] A tool is needed for high-yield strain screening and monitoring liquiritigenin in production, increasing the yield of liquiritigenin.

As a real-time, highly sensitive concentration detection element, a biosensor is just such a suitable tool. But biosensors that specifically and efficiently recognize liquiritigenin are not yet available. However, naringenin, a structural analog of liquiritigenin, can be efficiently identified by artificial biosensors in previous research, including transcription factors and riboswitches.[6] Based on this, we selected allosteric transcription repressor factor FdeR and a riboswitch that identify naringenin as starting points, and used error-prone PCR, site-directed mutagenesis, and phage-assisted continuous evolution strategies enabling them to specifically recognize naringenin.

LysR-type transcriptional regulators (LTTRs) are widely distributed in bacteria and can modulate promoter activity in prokaryotes. In this study, a native naringenin-responsive regulatory circuit from *Herbaspirillum seropedicae*, called the LysR-type PfdeAR-FdeR (promoter-TF) pair was coupled with a fluorescent protein to create a biosensor capable of converting liquiritigenin concentration into fluorescence intensity.[7] Subsequently, high-throughput screening was performed using a flow cytometer to obtain desired mutants. In vivo continuous evolution has the potential to significantly accelerate directed evolution, and a highly efficient phage-assisted continuous evolution (PACE) system constructed by Liu and co-workers, successfully evolving numerous proteins.[8] This system links the activity of the protein of interest (GOI) with the essential phage gene *gIII* expression, enabling the selection of mutants by promoting phage reproduction through the activation of GOI. This principle currently restricts its application in optimizing repressor-type transcription factors, with no reported use for such optimization. Therefore, we turned to another sensor element, the riboswitch,[6,9-12] which inherent

mechanism is allowed to be coupled with *gIII* expression and conducted continuous directed evolution.

In this study, based on allosteric transcription factors and riboswitches, liquiritigenin biosensors were evolved, which can translate intracellular liquiritigenin production into readily detectable biological signals, to construct a convenient biosensor toolkit for screening high-yield strains and dynamically-controlled liquiritigenin production pathways.

Result

2.1 Pathway design

In *H. seropedicae*, the binding of FdeR to naringenin relieves the inhibition of *fdeA*, the first gene of the FdeR operon responsible for naringenin degradation, enabling the strain to regulate the metabolism of naringenin.[7] As a basis of this study, pQE-80L-fdeR was designed and constructed, based on the reported sequences of the PfdeAR-FdeR native regulatory circuit from *H. seropedicae***.** The pathway consists of detection module and effect module (Figure 1 and Figure S12).[7,13,14] We conducted validation experiments for this pathway and fitted the Hill equation to the dose-response curves obtained from our measurements (Figure 2 and Figure S1, Table S4). The results demonstrated that this biosensor exhibited an increase in fluorescence intensity within 12 hours, gradually reaching a stable state. This biosensor exhibited measurable changes in fluorescence intensity in the concentration of naringenin within the range of 0-0.2 mM. However, within the concentration range of 0.2-0.5 mM, the wild-type FdeR showed a relatively stable response to naringenin, averaging at 6.5×10^6 a.u.. In contrast, its response to liquiritigenin remained consistently at a very low level across the entire concentration range. Moreover, we also measured the growth curves of wild-type FdeR to naringenin and liquiritigenin to determine the appropriate concentration range to ensure that both naringenin and liquiritigenin do not impact the normal growth of *Escherichia coli* **(***E. coli***)** (Figure S2). This confirms the feasibility of the screening pathway and demonstrates the optimized potential of the biosensor with FdeR as the detection module.

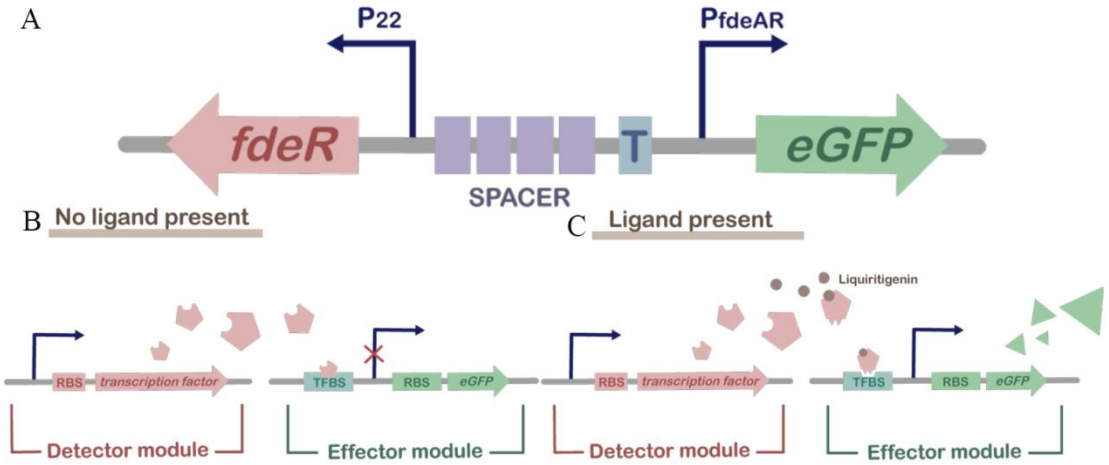

Figure 1. Schematic representation of the collection of synthetic FdeR biosensors.

(**A**) The detection module contains an artificial constitutive P22 core promoter and *fdeR*, while the effect module contains the bidirectional promoter PfdeAR with eGFP downstream of it. A random nonsense DNA spacer and terminator were inserted between P22 and PfdeAR so that transcription initiation by bidirectional promter PfdeAR in the *fdeR* direction was blocked to ensure a clear division of the two modules. (**B**) In the absence of liquiritigenin, FdeR can bind to PfdeAR to inhibit the expression of eGFP. (**C**) In the presence of liquiritigenin, FdeR binds to liquiritigenin causing its conformation changes, thus relieving the inhibition of eGFP.

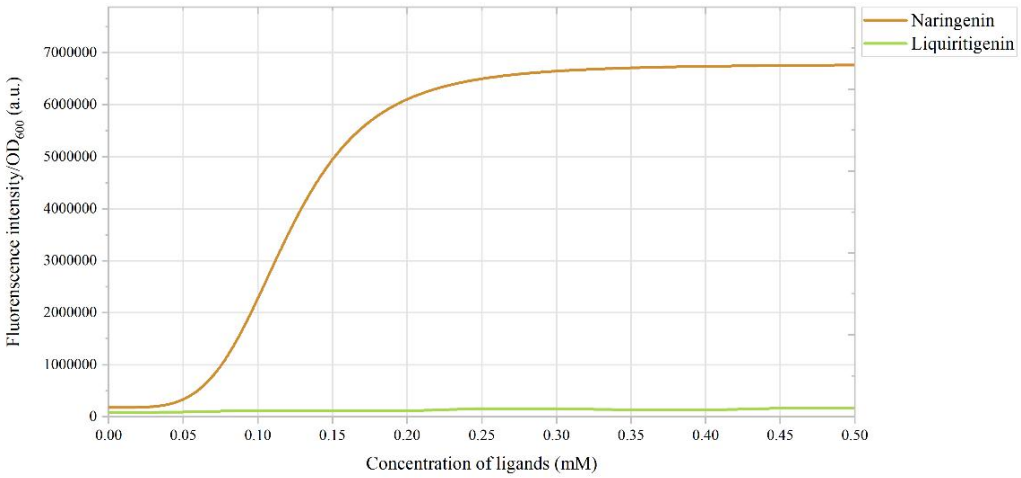

Figure 2. The dose-response curve of wild-type FdeR to naringenin and liquiritigenin. The orange curve represents the dose-response of wild-type FdeR to naringenin, while the green curve represents the response of wild-type FdeR to liquiritigenin.

Mutation libraries were established using two strategies: error-prone PCR (epPCR) and site-directed mutagenesis. two rounds of epPCR targeting the *fdeR* gene

with the StarMut Random Mutagenesis Kitt, constructing a mutation library of 5.9×106 mutants. Optimization of the PCR ion environment via gradient experiments resulted in a stable epPCR system with an appropriate mutation rate, ranging from 5 ~ 22 mutation bases per kilobase (kb) (Table S5).

Meanwhile, site-directed mutation was performed on the *fdeR* gene through seamless cloning, creating five combinations of mutation sites. Based on the known amino acid sequence of FdeR,[15] the three-dimensional (3D) structure of FdeR was predicted using AlphaFold2[16] (Figure S3A, S4A, and B). AutoDock 4.2.6[17] was employed to explore potential liquiritigenin binding sites on FdeR (Figure S4C, D, and E). Following energy minimization principles, the optimal docking result was selected from 50 docking results, demonstrating hydrogen bond interactions between FdeR's Arg220, Thr244, and Leu268 and liquiritigenin (Figure 3A and B). Besides, the docking analysis of FdeR and promoter indicated liquiritigenin is unlikely to cause steric hindrance with DNA (Figure S5). The binding energy of this conformation was within an reasonable range, justifying its selection for site-directed mutation. Subsequently, a full mutation scanning on amino acids within 3 Å of liquiritigenin identified mutations L268W, H170Y, and H170W (Table 1).[18] Containing five mutation combinations: L268W, H170Y, H170W, L268W + H170Y and L268W + H170W, the site-directed mutation library was transformed into *E. coli BL21* for subsequent fluorescence screening experiments.

Table 1. Main characteristics of FdeR single mutation prediction

Index	Mutation	Mutation Energy (kcal/mol)	Effect
1	A:HIS170>TRP	-0.83	STABILIZING
2	A:LEU268>TYR	-0.73	STABILIZING
3	A:HIS170>TYR	-0.57	STABILIZING

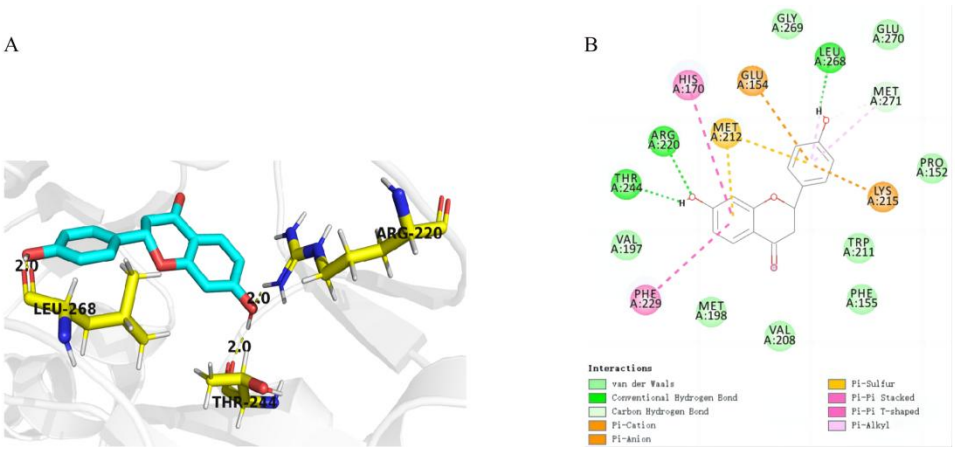

Figure 3. (**A**) Hydrogen Bond Contacts between FdeR and liquiritigenin. Amino acid residues on FdeR that form hydrogen bond contacts with liquiritigenin are labeled and represented using ball-and-stick models. Yellow dashed lines represent hydrogen bonds, and the numbers labeled above indicate the bond lengths. (**B**) Interactions between FdeR and liquiritigenin, including hydrogen bonds and various π bonds, as well as the bond lengths for each type of bond.

2.3 Mutants screening and fluorescence assay

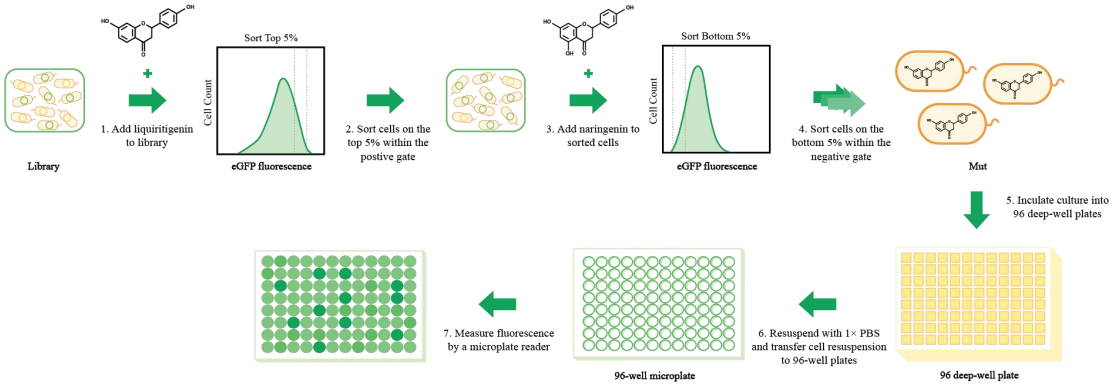

Figure 4. Flow chart of mutant screening and fluorscence assay. (**1**) Add liquiritigenin to library; (**2**) Sort cells on the top 5% within the positive gate; (**3**) Add naringenin to sorted cells; (**4**) Sort cells on the bottom 5% within negative gate; (**5**) Inculate culture into 96 deep-well plates; (**6**) Resuspend with 1× PBS and transfer cell resuspension to 96-well plates; (**7**) Measure fluorescence by a microplate reader.

With a sorting rate of up to 70,000 events per second, FACS technology was applied to screening for mutants that specifically and efficiently identify liquiritigenin to while having no or only low responsiveness to naringenin (Figure 4 and Figure S6). In the first round of epPCR, Six parallel epPCR systems were established for positive screening. Supplemented with 0.5 mM liquiritigenin and naringenin separately,

positive selections and negative selections were performed on the library (Figure 5A and B). Subsequently, 320 individual clones were used for 96-well microplate screening. This yielded a mutant library with a 2-10-fold increase in liquiritigenin response intensity compared to the wild type (Figure 6A). Among them, "Mut_49" stood out, displaying a remarkable 10-fold increase in peak fluorescence compared to the wild type. To further enhance the sensitivity and specificity of this biosensor in responding to liquiritigenin, we subjected four variants, namely Mut_39, Mut_49, Mut_58, and Mut_81, with favorable fluorescence characteristics to the next round of epPCR. Finally, “Mut_49_70” with a fluorescence intensity nearly 100 times higher than the wild type was isolated (Figure 6B), indicating a significant enhancement in this biosensor in responding to liquiritigenin.

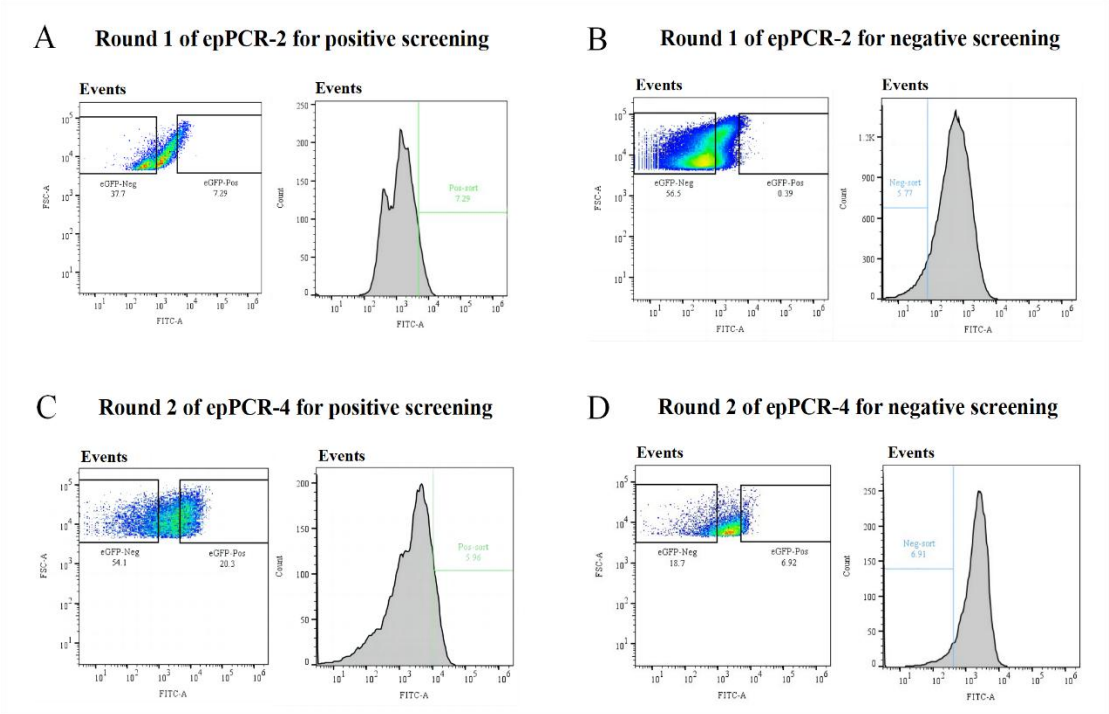

Figure 5. Flow cytometry analysis partly and FACS screening of the epPCR-2 and -4 library. Rounds of FACS screening were performed alternating positive sorting (library culture in the presence of 0.5 mM in the first round of epPCR or 0.35 mM in the second round of epPCR liquiritigenin and sorting of the events in the top of the histogram) and negative sorting (library culture in the presence of 0.5 mM in the first round of epPCR or 1.0 mM naringenin in the second round of epPCR and sorting of the events in the bottom of the fluorescence histogram). Round 1 of the epPCR library: (**A**) Positive screening was analyzed in a FCS-A vs. FITC-A scatter plot and the GFP Neg. (37.7%) and GFP Pos.

(7.29%) gates were set. An Events vs. FITC-A histogram plot was created and the Pos. Sort gate was delimitated to sort the 7.29% most fluorescent events. (**B**) Negative screening was analyzed in a FCS-A vs. FITC-A scatter plot and the GFP Neg. (56.5%) and GFP Pos. (0.39%) gates were set. An Events vs. FITC-A histogram plot was created and the Pos. Sort gate was delimitated to sort the 5.77% least fluorescent events. Rouns 2 of the epPCR library: (**C**) Positive screening was analyzed in a FCS-A vs. FITC-A scatter plot and the GFP Neg. (54.1%) and GFP Pos. (20.3%) gates were set. An Events vs. FITC-A histogram plot was created and the Pos. Sort gate was delimitated to sort the 5.96% most fluorescent events. (**D**) Negative screening was analyzed in a FCS-A vs. FITC-A scatter plot and the GFP Neg. (18.7%) and GFP Pos. (6.92%) gates were set. An Events vs. FITC-A histogram plot was created and the Pos. Sort gate was delimitated to sort the 6.91% least fluorescent events.

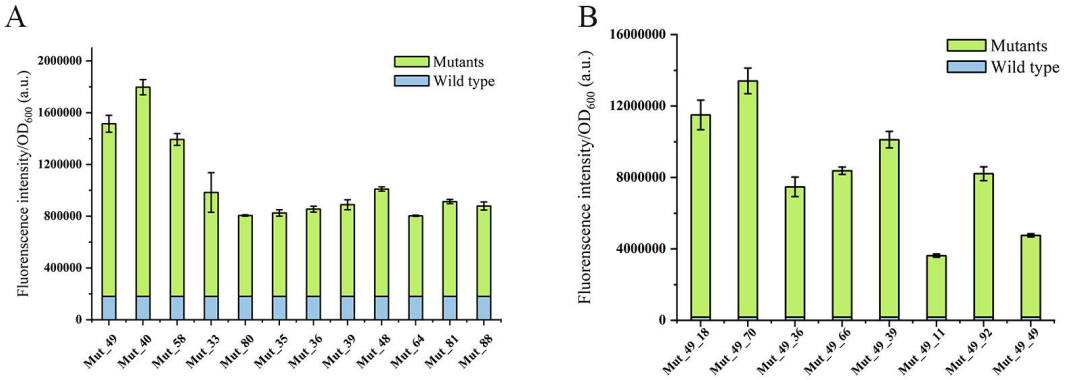

Figure 6. Comparison of the fluorescence intensities of mutants and the wild-type to liquiritigenin. (A) Mutants obtained from 1th error-prone PCR. **(B)** Mutants obtained from 2nd error-prone PCR. Mutants and wild-type were induced with 1 mM liquiritigenin for 12 hours. The green bars represent the fluorescence intensities of different mutants, while the blue bars represent the fluorescence intensity of the wild-type.

In site-directed mutation experiments, we performed a 96-deep well microplate screening with 1.0 mM liquiritigenin or 1.0 mM naringenin. Regrettably, the mutants exhibit no significant increase in response intensity to liquiritigenin or naringenin compared to the wild-type FdeR (Figure 7). Consequently, a dose-response analysis for these mutants was not conducted, necessitating a reevaluation of our bioinformatics-based predictions. R. Wassem *et al.* demonstrated[19] that FdeR recognizes and binds to the PfdeA promoter, inhibiting RNA polymerase access. Upon binding flavonoids, like naringenin, FdeR undergoes conformational

changes altering its DNA-binding site, enabling RNA polymerase binding and transcription initiation. Initial molecular docking focused on the individual FdeR monomer interaction with liquiritigenin, neglecting dynamic changes in FdeR binding to the PfdeA promoter and its oligomeric state in vivo. Future research will readdress this aspect through molecular docking to identify novel mutation sites.[19]

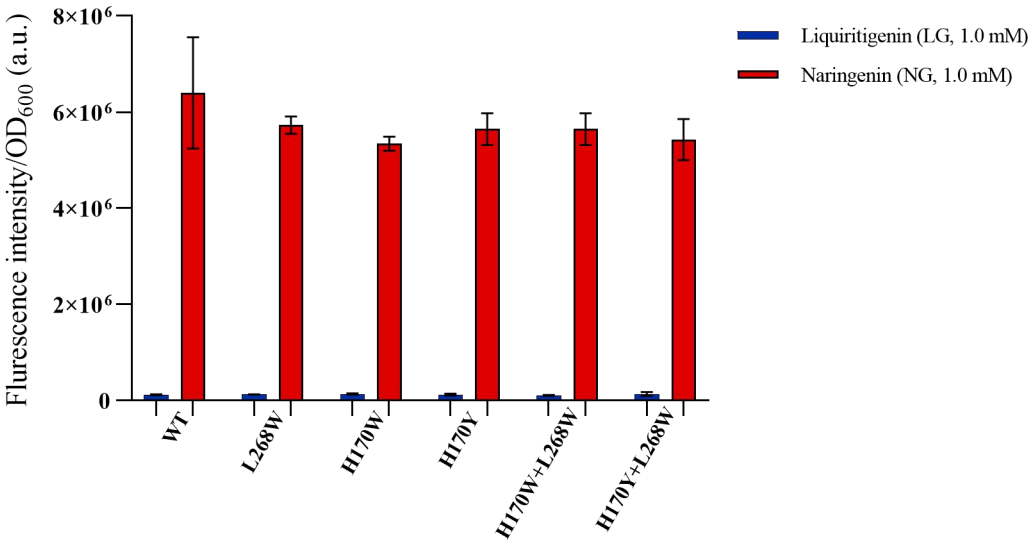

Figure 7. Dose responses to liquiritigenin and naringenin of different mutantgensis constructs. Wild-type (WT) and five combinations of mutantgensis L268W, H170Y, H170W, H170W + L268W, H170Y + L268W were cultivated for 12 h in the presence of increasing concentrations of liquiritigenin (blue) and naringenin (red) in 500 μM. Error bars are based on the standard deviation of a minimum of biological triplicate.

2.4 Performance testing of mutant PfdeAR-FdeR sensors

Based on the 96-well microplate fluorescence screening, 8 mutants with high fluorescence intensity responses to liquiritigenin were selected for gradient experiments, varying liquiritigenin concentration and induction time, to characterize their performance as biosensor, including sensitivity, detection range, response time, and specificity, modeled using Hill functions to analyze dose impact.[14] We defined operational range as the ligand concentration range and response intensity as fluorescence intensity divided by OD_{600}. We also introduced a *Noise* parameter to

quantify average relative error in fluorescence response across concentrations, a vital aspect in biosensor development and application.

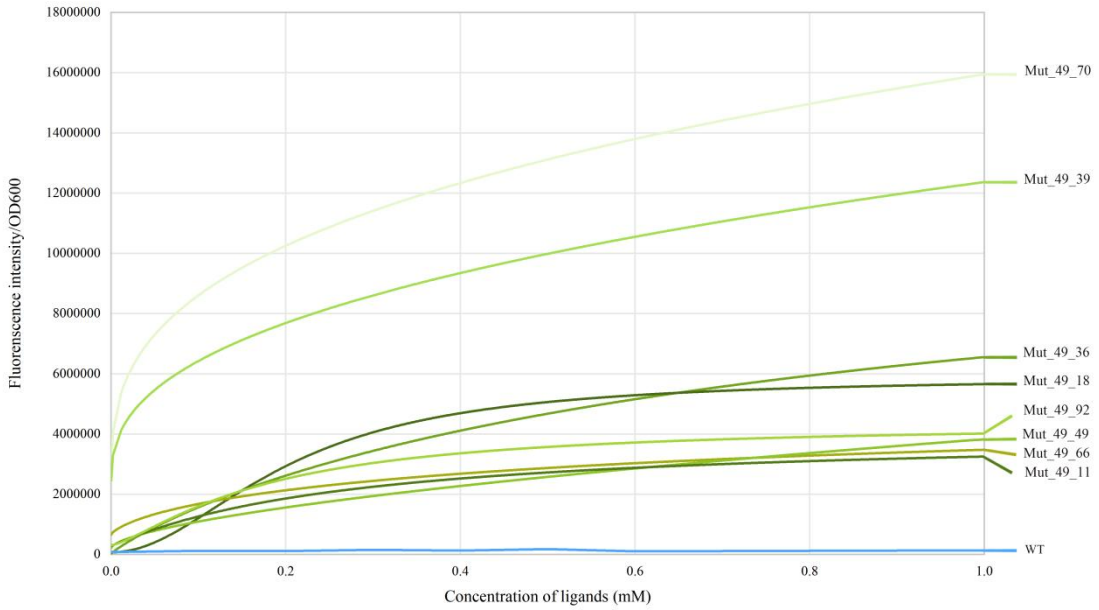

Figure 8. The dose-response curves for liquiritigenin of the wild type and the mutants are as follows: The blue curve represents the dose-response curve for the wild type. Various green curves represent the dose-response curves for the 8 mutants.

Compared to the initial state, all 8 mutants showed substantial 10-100-fold enhancements in fluorescence response intensity (Figure 6B), exhibiting a positive correlation within the 0-1 mM liquiritigenin concentration range, with most reaching a plateau at 0.5 mM liquiritigenin (Figure 8, Table S4). Notably, Mut_49_70 and Mut_49_39 exhibited more higher fluorescence intensity and a broader detection range. Even at 1 mM liquiritigenin, their response curves continued to show an upward trend, while *Noise* parameters both remained around 20% (Table S4). Next, the response time capabilities of the eight mutants were assessed (Figure 9). While the wild-type FdeR displayed an S-shaped time response curve, with fluorescence intensity increasing soomthly at approximately 6 hours and peaking at 10 hours, Mut_49_70 exhibited a significantly longer response time. It showed rapid early-stage intensity rise within 2 hours, reaching its peak at approximately 12 hours, indicating Mut_49_70 can respond quickly to liquiritigenin in the environment. To

evaluate specificity, we conducted dose-response experiments for naringenin in the 8 mutants (Figure 10A, B, C, and Figure S8). These mutants exhibited strong specificity, with most displaying over a 5-fold difference in response intensity to liquiritigenin compared to naringenin. Notably, Mut_49_70 showed the highest fluorescence intensity among the mutants, exceeding 1.7×10^7 a.u.. However, its response intensity to naringenin also ranked the highest, reaching approximately 2.1×10^6 a.u. (still lower than wild-type FdeR). And Mut_49_39 exhibited impressive fluorescence response intensity, reaching up to 1.2×10^7 a.u., with significantly stronger specificity for liquiritigenin than Mut_49_70. Mut_49_39 displayed a broader dynamic range, maintaining an upward trend in fluorescence intensity even at a 1.0 mM liquiritigenin concentration, which is often considered as an ideal characteristic for a biosensor.

Additionally, We identified mutations, including D71E, S140P, M191T, and S297C, enriched in most mutants. Remarkably, elongation mutations were observed in Mut_33, Mut_48, Mut_49, and Mut_64, enhancing their responsiveness and specificity to liquiritigenin (Figure 11 and 6). Compared to Mut_49, F106L and V134L mutations enriched in Mut_49_75, Mut_49_77, Mut_49_78, Mut_49_18, and Mut_49_36, while E163V and I308S mutations were enriched in Mut_49_40 and Mut_49_41. And Mut_49_39 and Mut_49_70 showed no additional mutations, but an mutation (G to A) was detected between the promoter and RBS, potentially influencing biosensor performance at the transcriptional or translational level, resulting in both mutants constructing the best-performing biosensors. These sequencing results serve as the foundation for subsequent molecular dynamics simulations.

In summary, among the 8 mutants studied, Mut_49_39 and Mut_49_70 demonstrated a broader response range (exceeding 1 mM), faster response kinetics (within 2 hours), and a relatively normal Noise parameter (about 20%). Consequently, Mut_49_39 and Mut_49_70 hold substantial potential for constructing highly efficient and specific liquiritigenin biosensors.

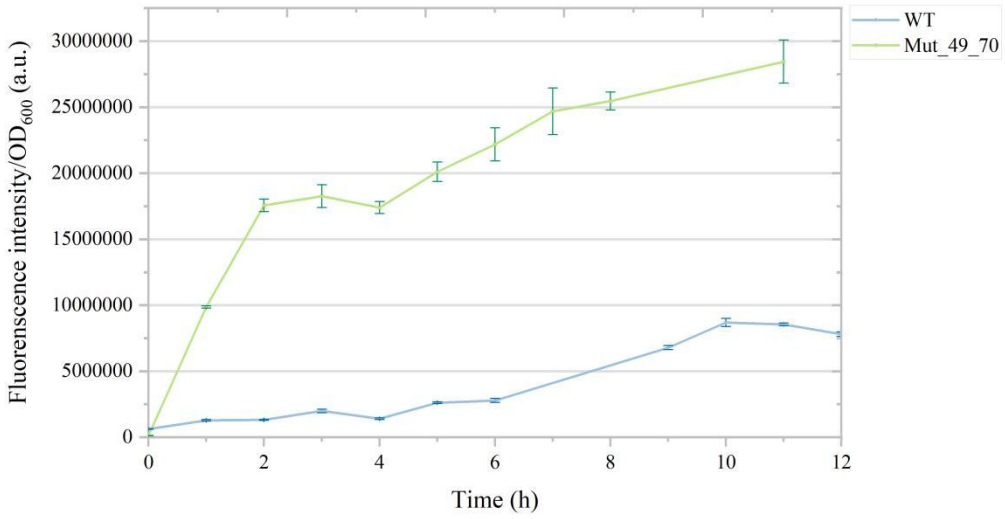

Figure 9. The response time curves for liquiritigenin of the wild type and Mut_49_70 are as follows: The blue curve represents the response time curve for the wild type. The green curve represents the response time curve for the mutant Mut_49_70.

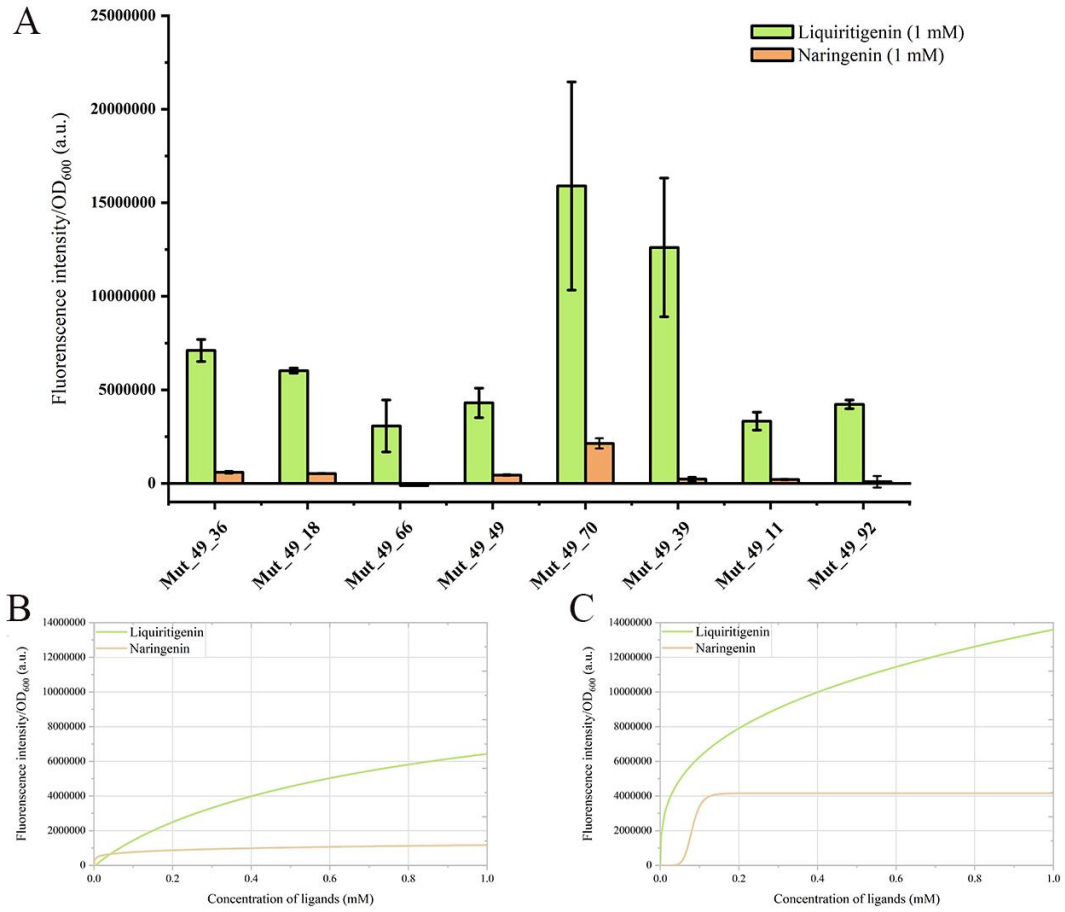

Figure 10. Fluorescence intensities of different mutants to liquiritigenin and naringenin. **(A)** Fluorescence intensities of 8 mutants to 1 mM liquiritigenin and naringenin induction, where green bars represent the liquiritigenin, and orange bars represent the naringenin. **(B)** The dose-response curves of the Mut_49_36 mutant to liquiritigenin and naringenin. **(C)** The dose-response curves of the Mut_49_70 mutant to liquiritigenin and naringenin**.** The green curve represents liquiritigenin, and the orange curve represents naringenin in the dose-response curves for both ligands.

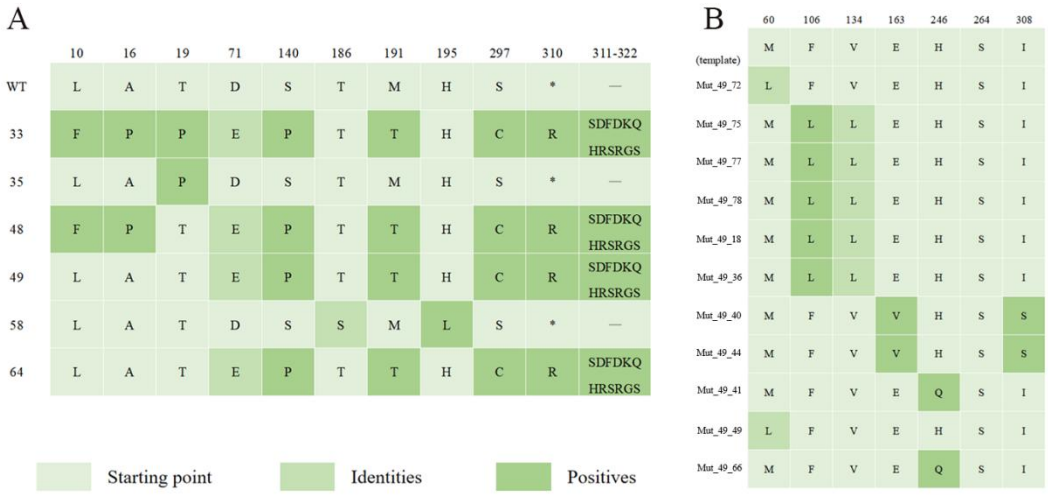

Figure 11. **The amino acid mutation heatmap of the mutants.** (**A**) After the first round of error-prone PCR, six mutants were identified. Among them, four mutants exhibited enrichment in mutations at S140P, M191T, and S297C, and leading to extended mutations spanning twelve amino acids. (**B**) The mutants obtained after the second round of error-prone PCR, using Mut_49 as a template, were sequenced and analyzed. Mutations enriched in F106L and V134L were observed when compared to the Mut_49 template.

2.5 Docking and Molecular Dynamic Simulations

After predicting the three-dimensional structure of Mut_49, this mutant was docked with liquiritigenin, analying changes in intermolecular forces and binding pocket hydrophobicity (Figure S9 and 10). The results indicated that Mut_49 revealed higher hydrophobicity in the binding region compared to the wild-type, suggesting enhanced affinity and specificity for liquiritigenin. Unfortunately, upon analyzing its

mutation energy, it was found that all mutations were neutral, contradicting the experimental results (Figure 12).

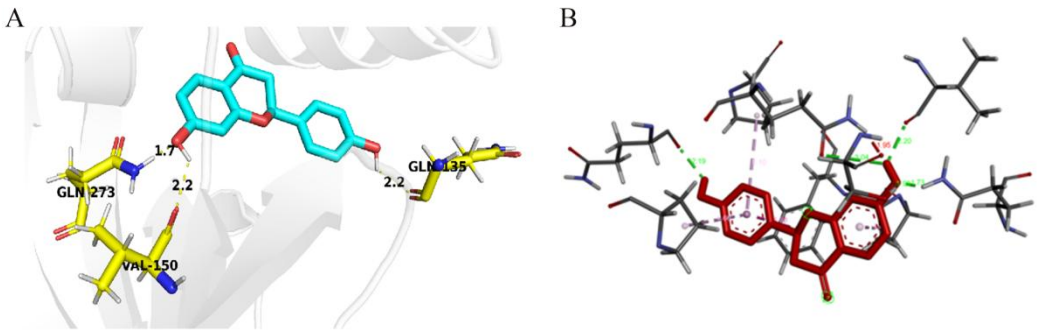

Figure 12. (A) Hydrogen bond interactions between mutant 49 and liquiritigenin. Liquiritigenin and the amino acid residues of mutant 49 that have hydrogen bond interactions are labeled and shown in ball-and-stick model. Yellow dashed lines represent hydrogen bonds, and the numbers on them indicate the hydrogen bond lengths. **(B)** The intermolecular forces between mutant 49 and liquiritigenin, such as hydrogen bonds and various π bonds, and the bond lengths of each type of bond.

Table 2. Main characteristics of mutant 49 mutation prediction

Index	Mutation	Mutation Energy (kcal/mol)	Effect
1	A: VAL134>LEU	0.05	NEUTRAL
2	A: PHE106>LEU	0.07	NEUTRAL
3	A: PHE106>LEU A: VAL134>LEU	0.07	NEUTRAL
4	A: MET60>LEU	0.00	NEUTRAL
5	A: HIS246>GLU	0.41	NEUTRAL

We then carried out molecular dynamics simulations on the complexes of FdeR with liquiritigenin and mutant 49 with liquiritigenin, respectively.[20] The structural changes and the binding between WT and liquiritigenin were investigated by viewing the system potential energy, Rg, RMSD, and interaction energy (Figure 13). MMPBSA analysis was carried out to correlate the MD data with peptide characteristics (Table 3). The interaction energy of the WT was about 15% lower than that of MU, demonstrating that the binding affinity between the WT and the receptor was much higher than the mutant type.

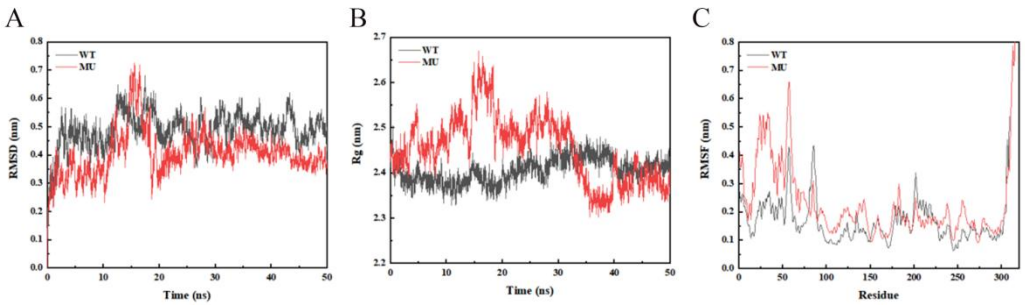

Figure 13. Molecular dynamics trajectory analysis of WT and mutant 49. WT stands for FdeR and MU stands for mutant 49. (A) The RMSD curve of the protein during the protein-ligand complex simulation process (the complex reached equilibrium after 20 ns, indicating that the whole simulation process was stable and reliable); **(B)** The Rg curve of the protein during the protein-ligand complex simulation process (the radius of gyration (Rg) is used to prove the compactness of the protein structure during the simulation process, it is the distance between the centroid of all atoms and their ends at a specific time interval. During the whole complex MD simulation process, the Rg value fluctuation of MU was larger than that of WT, indicating that WT might bind more tightly with the small molecule); **(C)** The RMSF curve of the protein during the protein-ligand complex simulation process (the fluctuation of each atom relative to its average position is calculated, which characterizes the average of the structural changes over time, and gives a characterization of the flexibility of each region of the protein. The RMSF value of the protein in the MU-ligand complex group was larger than that of the protein in the WT-ligand complex group in the 0-75 range, indicating that the flexibility of MU was greater than that of WT).

Table 3. Comparison of statistics between WT and MU

Energy	WT	MU
Van der Waals Energy (KJ/mol)	-156.689	-131.048
Electrostatic Energy (kJ/mol)	-29.978	-7.192
Polar solvation Energy (KJ/mol)	101.397	67.802
Nonpolar solvation Energy (KJ/mol)	-16.180	-17.227
Total Binding Energy (KJ/mol)	-101.451	-87.666
TΔS(KJ/mol)	4.444	10.645
Total Binding Free Energy (KJ/mol)	-97.007	-77.021

Note: In order to better explain the interaction energy between the protein and the ligand, we used the

gmx_mmpbsa script (https://jerkwin.github.io/gmxtool/) to determine the binding energy of all the protein-ligand complexes at the equilibrium stage. In the MMPBSA method, the total binding energy is decomposed into four independent parts (electrostatic interaction, van der Waals interaction, polar solvation and non-polar solvation interactions).

2.6 Riboswitches directed evolution via phage-assisted continuous evolution (PACE)

The expression of transcription factor-based biosensors affects the performance of biosensors as they place an unnecessary burden on the cell and are subject to trans-regulatory mechanisms,[21] leading to delayed protein responses and off-target effects. Imposing less metabolic burden on cells, riboswitches are excellent sensing elements, as they undergoes conformational changes to regulate the expression of downstream genes, after binding to specific molecules with high affinity and specificity. Fluorescence intensity is influenced by external factors such as bacterial growth conditions and complex manual operations, limiting its stringency as a screening metric. Therefore, there is an attempt to find a high-throughput and time-efficient continuous directed evolution strategy.

In 2011, David R. Liu introduced a high-throughput in vivo protein continuous directed evolution system called Phage-Assisted Continuous Evolution (PACE).[22] The PACE system has a broad range of applications, and theoretically, any protein that can be coupled with the activity of the pIII can serve as an evolutionary target. This includes proteins such as proteases,[8] Bt toxins,[23] aminoacyl-tRNA synthetases,[24] and more. During the PACE process, induced by various mutagenic genes on the mutagenesis plasmid MP,[25] mutation rate increase dramatically across the entire genome of *Escherichia coli*. Only phage containing desirable mutated genes can effectively activate the expression of the *gIII*, allowing the phage to propagate normally and stably exist in the lagoon. Conversely, undesirable mutant phage cannot replicate normally and are excluded from the lagoon.

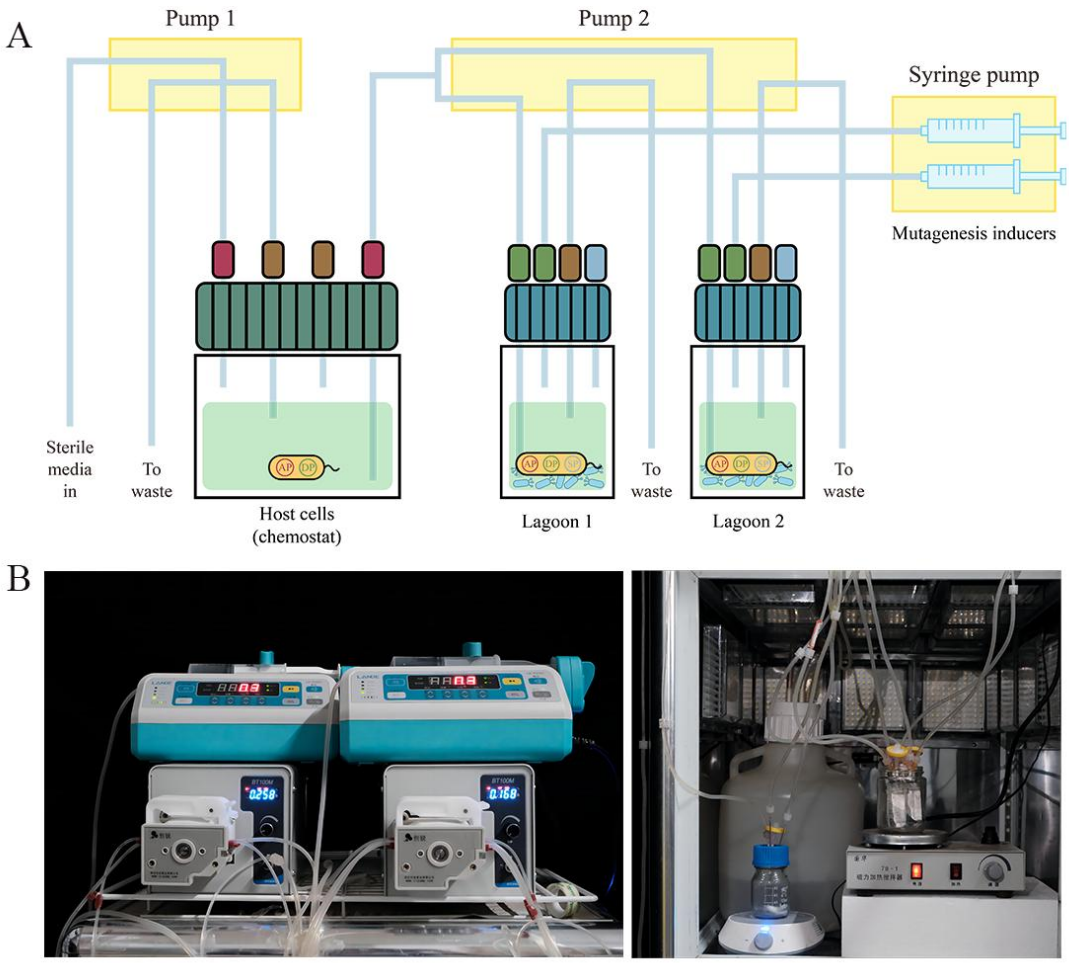

Figure 14. (A) Schematic of the PACE apparatus. Coupled to each other, allowing the phage to continuously cross-seed between the two lagoons. Chemostat. Provide constant cell density for lagoons for M13 bacteriophage infection. Lagoons, Phage infect and propagate. Inducers. Initiate the expression of mutagenic genes to mutate at the genome-wide level of *E. coli.* **(B)** Photo of our PACE apparatus. The picture on the left shows syringe pumps and peristaltic pumps. The picture on the right shows DRM carboy, the chemostat and lagoons.

Given this characteristic, riboswitches can be effectively coupled with PACE. Yoo Yeol Jung and colleagues designed artificial synthetic naringenin riboswitches, Mid and High, using a combination of SELEX and in vivo screening methods (Table S7).[6] Among the two of them, Mid can respond to moderate concentrations of naringenin (approximately 100 mg/L), while High can respond to high concentrations of naringenin (approximately 200 mg/L). We selected two mutants, Mid2 and High2, as our starting points for evolution. Therefore, we designed a specific PACE system allowing the continuous directed evolution of riboswitches through both positive and

negative selection pathways (Figure 14A and 15). In the positive selection, if the ideal mutant binds to liquiritigenin, allowing T7 RNA polymerase to be translated normally, thus T7 RNA polymerase can initiate *gIII* expression, and enable the phage to propagate normally. The activity of mutants can be reflected by eGFP expression. To obtain mutants with higher activity, selection pressure was gradually increased by reducing the concentration of anhydrotetracycline. For the negative selection, pIII-neg, a dominant negative mutant of pIII, was used to impair the infectivity of newly born phages.[26] When adding naringenin instead of liquiritigenin, if the mutant responds to naringenin, T7 RNA polymerase can be translated normally and activate *gIII-neg* expression. Even with *gIII* expression, the phage cannot propagate properly. After positive and negative selection, the riboswitch's affinity for liquiritigenin was enhanced, while its binding capability for naringenin was decreased.

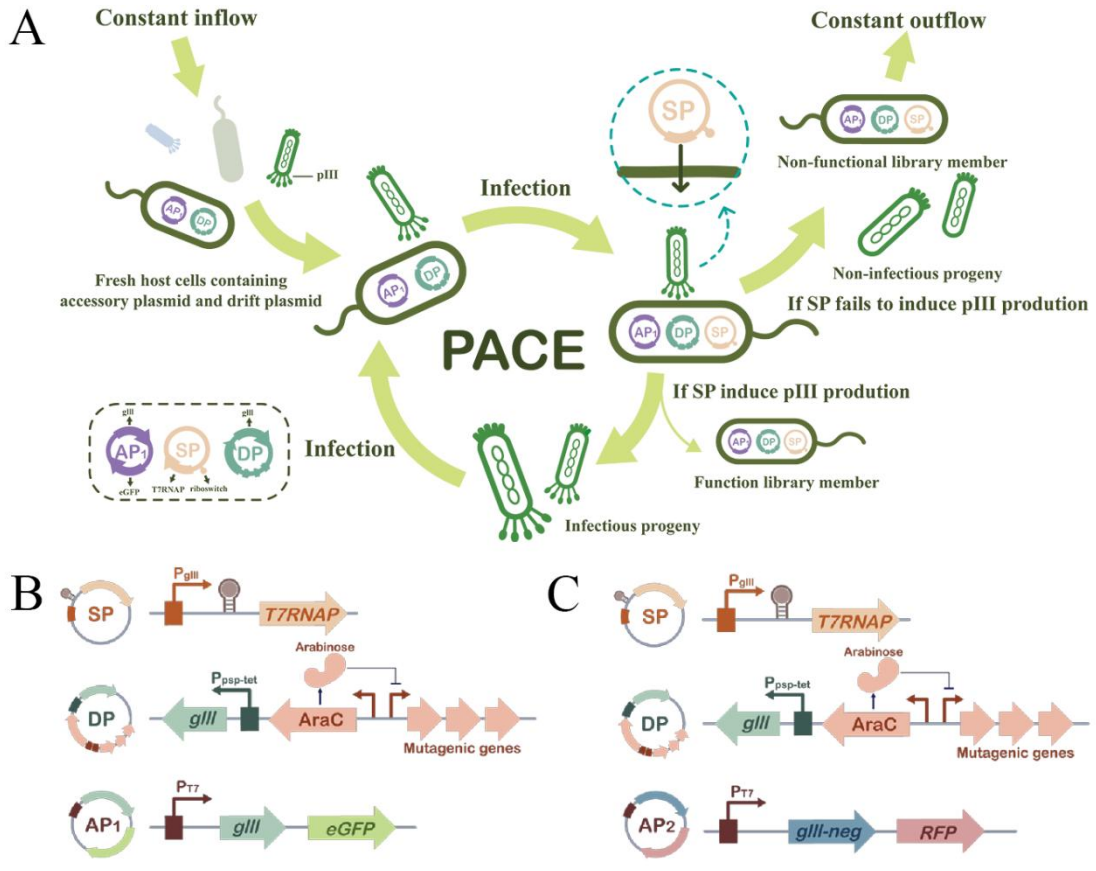

Figure 15. PACE positive and negative screening pathway. (A) Host cells flow continuously in the lagoon and are infected here by selection phage (SP) containing mutant library. Functional library members bind liquiritigenin and initiate transcription of the downstream T7 RNAP gene on SP, which ultimately allows the AP to produce pIII and release

progeny capable of infecting new host cells, whereas non-functional library ones do not. Random mutations occur in all genes of the host cell and phage under the induction of drift plasmid (DP). And since host cells replicate more slowly than the lagoon flow, any host cells that accumulate mutations in the plasmids or genome are excluded from the lagoon. Besides, the expression of *gIII* on the DP will be initiated when anhydrotetracycline is added, which can reduce the stringency of selection. Gradually reducing the concentration of anhydrotetracycline increases the selection pressure. **(B)** Positive selection. Positive screening couples the transcription of T7 RNAP to *gIII* expression. If riboswitch binds liquiritigenin, T7 RNAP is transcripted normally. Thereby T7 RNAP activates the expression of the T7 promoter-controlled *gIII* on the AP. **(C)**Negative selection. When undesirable riboswitch binds naringenin in the negative selection, it activates *gIII-neg* expression, which hinders the infectivity of the progeny phage. In the absence of undesirable bind, the *gIII* expresses and the phage reproduce normally. The screening pressure of the negative selection is regulated by the concentration of anhydrotetracycline (ATc).

Currently, we have successfully constructed the plasmids (SP, AP and CP) required for PACE (Figure 16, Figure S13,S14). We also successfully built the PACE device, tuned the operational parameters of syringe pumps and peristaltic pumps, as well as the length of needles in the chemostat and lagoons(Figure 14). This ensured the host bacteria maintained a stable cell density and allowed M13 phage propagate normally in the lagoons.The mutation rate μ_{bp} of DP6 has been measured as 1.007×10^{-5}, and the PACE system has been initiated. We will isolate promising individuals from this pool and further test their performance as biosensors.

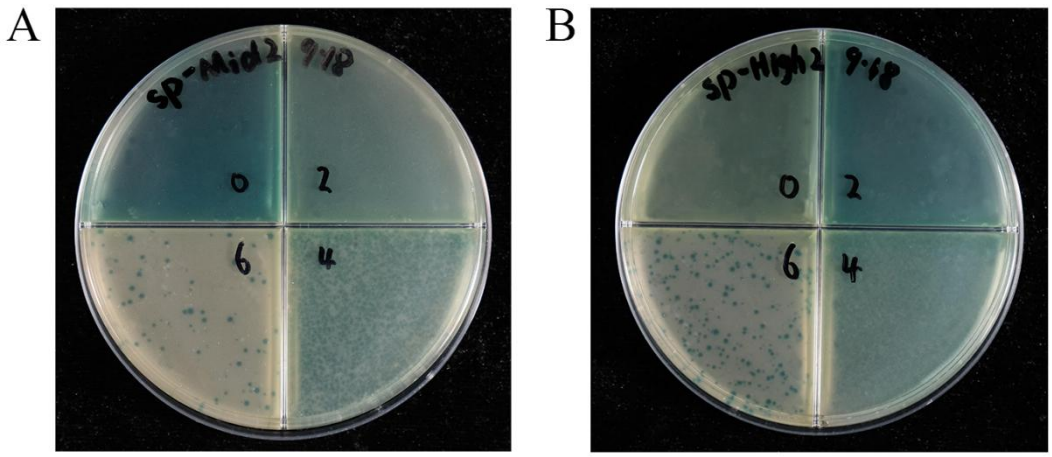

Figure 16. Activity-independent phage plaque assay. (A) SP-Mid2 phage and **(B)** SP-High2 phage; from the upper right quadrant, upper left quadrant, lower right quadrant, and lower left quadrant, the phage concentrations are 10^{0}, 10^{-2}, 10^{-4}, 10^{-6} in order, and the number of phages in appropriate in quadrants can be used to quantify the titer.

Discussion

Allosteric transcription factors (aTFs), as a type of controllable regulatory proteins, can find extensive applications in synthetic biology research. In the present work, a novel liquiritigenin-responsive biosensor based on aTFs has been developed. Focusing on the PfdeAR-FdeR fluorescent screening pathway, we demonstrated the feasibility of altering the specificity ligand of the transcription factor FdeR through directed evolution, resulting in a 10 to 100-fold increase in its ability to specifically bind liquiritigenin. Based on transcription factors and riboswitches, our research contributes to large libraries of FdeR biosensor mutants responding to liquiritigenin. The resulting mutants possesses functional and biochemical characteristics, and further mutations are introduced to explore the effects of amino acid changes on biosensor performance.

Application of PACE system in multiple pathway and parallel screening is limited by its complex continuous culture apparatus and necessary process control. To achieve multiple screening simultaneously and in parallel, Liu and his colleagues combined the EvolvR technology with PACE.[27] Meanwhile, a recently published

sPACE strategy[28] is also an excellent method to increase the number of evolution experiments that can be performed in parallel. We will try to apply the above strategy to the directed evolution of riboswitch High2 and Mid2, to construct a multi-system parallel directed evolution system.

We found discrepancies between our bioinformatics predictions and experimental results. This could be the reason of AlphaFold2's inability to distinguish protein monomers and multimers. We presumed FdeR was a monomer, but it might be a multimer in vivo, affecting the subsequent experiments. Moreover, we choose the fifth-ranked docking conformation as the best one, matching the experimental data. However, this conformation had an implausible hydrogen bond energy, with a hydrogen acceptor and two oxygen donors. This might also affect the molecular dynamics simulations.

Additionally, promoter and plasmid copy number engineering affect the biosensor performance at the transcription level, while RBS modification controls the transcription factors and reporter proteins at the translation level, regulating the biosensor response curve. Therefore, to further improve the response range, speed, and specificity of liquiritigenin biosensors, we will consider rational design methods such as deep learning to optimize the genetic circuits.[29]

In summary, we have developed a liquiritigenin biosensor based on aTFs for the first time. It exhibits significant improvements in sensitivity, detection range, and specificity compared to the wild-type, with a 10 to 100-fold increase. Our work provides a new approach for flavonoid metabolic engineering and serves as a methodological reference for the development of flavonoid biosensors. We hope that this biosensor could serve as a new tool for intracellular detection of liquiritigenin synthesis, contribute to the regulation and optimization of the microbial synthesis pathway of liquiritigenin. By using FACS to select high-yield liquiritigenin strains from a vast pool of variants, a high-throughput screening system for metabolite response can be established, greatly increasing the yield of liquiritigenin microbial

synthesis. In addition, our work also extends the application of PACE to riboswitch evolution, providing new ideas for the evolution of riboswitches. In the future, we envision that the biosensor toolkit can help the evolution of small molecule production and guide the construction and optimization of cell factories.

Materials and Methods

1. Strains and Plasmids

All strains and plasmids used in this study are listed in Supplementary Table S1 and Table S2, respectively. *E. coli DH5α* (Vazyme, Nanjing, China) was used for recombinant DNA manipulation. *E. coli BL21(DE3)* (Vazyme, Nanjing, China) was used as the host for biosensor validation. *E. coli S2060* was purchase from Addgene[30] (Addgene, cat. no. 105064). The plasmid pJC175e was transformed into *E. coli S2060* to obtain *E. coli S2208*. These two strains were mainly used in the PACE experiment.

The biosensor parts with the gene for *fdeR* and *eGFP*, the promoters P22 and PfdeR were commercially synthesized by General Biol. And naringenin riboswitches of Mid2 and High2 were also synthetized by General Biol. The vector pQE-80L was used as the basis for the biosensor in this experiment and was from the laboratory of Professor YanXin, Nanjing Agricultural University.The pJC175e (Addgene plasmid # 79219), pBT137-splitC (Addgene plasmid #122605), pBT137-splitD (Addgene plasmid # 122606), DP6 (Addgene plasmid #140446) and AP-T7P plasmids were purchased from Addgene.[23]

2. Chemicals and Strain cultivation

Authentic standards of naringenin and liquiritigenin were purchased from Macklin Biochemical Technology (Shanghai, China) and **Chengdu Lemeitian Medicine Science And Technology** (Sichuan, China). Stocks were prepared dissolving the naringenin and liquiritigenin in dimethyl sulfoxide (DMSO) at the concentration of 0.5 M and 20 mM, respectively *E. coli DH5α* and *E. coli BL21* were grown at 37°C in Luria−Bertani broth (LB) medium containing the appropriate antibiotics (50mg/L kanamycin) when required. In a PACE experiment, 2×Yeast Extract and Typeptone (2×YT) medium (Solarbio, Beijing, China) was used to cultivate *E. coli S2060* and *E.* coli S2208 and was used for activity-independent phage plaque assay. Davis Rich Media (DRM)[22] was used to maintain the operation of the PACE system by supplementing with antibiotics (25 mg/L chloramphenicol, 50 mg/L ampicillin, 50 mg/L streptomycin) when required.

All oligonucleotide primers used to amplify DNA fragments are shown in Tables S2 and S3, respectively, was used to obtain the linearized vector and DNA fragment by PCR reaction.

PCR was carried out using 2 × Phanta Max Master Mix (Dye Plus) (Vazyme, Nanjing, China) according to manufacturer's instructions. The PCR products were verified by electrophoresis and purified using a FastPure Gel DNA Extraction Mini Kit (Vazyme, Nanjing, China). DNA fragments assembly were performed by ClonExpress II One Step Cloning Kit (Vazyme, Nanjing, China). *E. coli DH5α* and *E. coli BL21* were conducted according to the standard heat shock

method. Besides, *E. coli S2060* transformation followed the experimental method of Liu's work.[31] Plasmids were isolated using a FastPure Plasmid Mini Kit (Vazyme, Nanjing, China).

3. Error-Prone PCR of the *fdeR* gene

Using the error-prone PCR kit (Gene-star company) in a total volume of 25 μL using template 10 ng of pQE-80L-fdeR plasmid as template , 10μL 2×StarMut Random PCR Mix , 10 mM Gen 2-F, 10 μM Gen 2-R each, Star Mut enhancer 6 μL, sterile water was made up to 25 μL, 53.1℃) or error-prone PCR on *fdeR* fragments. Subsequently, the above *fdeR* gene fragments were sequenced by Sanger Sequence. Then based on the sequencing results, the number of mutated bases per thousand bases was calculated. Meanwhile, the linearized vector and the above fragments were assembled by ClonExpress II One Step Cloning Kit (Vazyme, Nanjing, China). *E. coli BL21* was used for subsequent chemical transformation.

4. Site-Directed Mutation of FdeR

For construction of the single and double mutants of fdeR, the template the pQE-80L-fdeR plasmid was used along with a suitable combination of primers(Table S3).Three pairs of primers were designed to introduce three mutations (H170W,H170Y,L268W) on two sites in FdeR. The whole pQE-80L-fdeR plasmid was divided into two or three parts and then amplified by two or three pairs of primers(Table S3). The consequent two or three fragments with introduced mutations were combined with ClonExpress II One Step Cloning Kit or ClonExpress MultiS One Step Cloning Kit (Vazyme, Nanjing, China), which is a cloning kit based on homologous recombination. *E.coli DH5α* was used for subsequent chemical transformation. The plasmids from individual transformants were used to DNA sequence to confirm that correct mutation was obtained. Than, plasmids with correct mutations were transformed into *E.coli BL21*. Randomly select individual colonies for fluorescence screening.

5. Fluorescence activated cell sorting (FACS) and 96-well plates screening

Cultures of *E. coli BL21* with empty pQE-80L plasmids (Negative control) or transformed with plasmids containing eGFP reporter (Positive control). Library of FdeR mutants were grown overnight in 5 ml LB medium supplemented with 50 mg/mL kanamycin which grown on a biological shaker for 12 h at 220 rpm and 37℃. Cultures were diluted (1:100) into fresh media, grown until OD_{600}~0.6 and induced with 0.5 mM liquiritigenin for 12 h.

The culture was diluted 10-fold in fresh liquid LB medium and analysed using FACS (BD FACSAria III, Institute of Soil Science, Chinese Academy of Sciences). A histogram plot was generated by sorting cells with empty pQE-80L plasmids and defining a negative gate as negative control. Meanwhile, using cells with plasmids containing eGFP reporter to designate a positive gate as a postive control (Figure S6). Two rounds of FACS counter-selection were constructed with liquiritigeni induction or naringenin induction.

In the 1st round, positive sorting was performed, collecting the population on the top 5%~10% of the histogram plot under the positive gate. At least 2.4×10^7 events were analysed by the flow cytometer, which can cover entire experimental libraries(5.6×10^6). The collected cells

were added into 5ml liquid LB medium supplemented with kanamycin to grow at biological shaker 220 rpm, 37℃, overnight. Cultures were diluted (1:100) into fresh LB medium, grown until OD_{600}~0.6 and induced with 0.5 mM naringenin for 12 h as the samples of 2nd round (Figure S7).

In the 2nd round, negative sorting was performed, collecting the population on the bottom 5%~10% within the negative gate. At least 4.1×10^6 events were passed through the flow cytometer corresponding to 10-fold the initial library size. The sorted cells were plated on LB agar meium supplemented with 50 mg/mL Kanamycin overnight. Colonies were used for subsequent 96-well plates screening.

6. 96 deep-well plates screening

The bacterial solution in 96 deep-well plate was centrifuged at 4000 rpm for 8 min after the induction culture completed, and then discard the supernatant. 1000 μL cold PBS buffer per well was pipetted and resuspended, and 200μl was taken into a 96-well fluorescent plate. Use a microplate reader to measure the fluorescence at Ex = 482 nm/Em = 524 nm and the absorbance at OD_{600}.

7. Characterization and compensation test of biosensor

A concentration gradient of liquiritigenin ranging from 0 to 1 mM was introduced into 1 mL of bacterial culture containing kanamycin in a 96 deep-well plate, supplemented with 0.5 mM naringenin. The well-characterized variants were introduced into 5 mL of LB medium with kanamycin and incubated overnight at 37°C and 220 rpm on a shaker until reaching saturation. Plasmids were extracted using the FastPure Plasmid Mini Kit (Vazyme, Nanjing, China) and subsequently retransformed into *BL21*(*DE3*) competent cells (Vazyme, Nanjing, China). These cells were inoculated into 5 mL of kanamycin-supplemented LB medium and grown overnight on a Biological Shaker at 220 rpm and 37°C. Following cell resuspension, fluorescence intensity was measured using a microplate reader.

8. Data Processing and Statistical Analysis

When measuring fluorescence, we used 1×PBS to correct for background fluorescence and optical density of the PBS (FP_{PBS} and OD_{PBS}, respectively) for each imposed naringenin or liquiritigenin concentration. The normalized fluorescence for optical density was calculated as follows:

$$\left(\frac{\mathrm{FP}}{\mathrm{OD}}\right)_{\mathrm{cor}} = \frac{\mathrm{FP} - \mathrm{FP}_{\mathrm{PBS}}}{\mathrm{OD} - \mathrm{OD}_{\mathrm{PBS}}}$$

The resulting mean $\left(\frac{\overline{\mathrm{FP}}}{\mathrm{OD}}\right)_{\mathrm{cor}}$ each concentration of naringenin or liquiritigenin, are expressed in arbitrary units (a.u.) and were fitted with the Hill function as follow using the weighted nonlinear least-squares algorithm (curve_fit, SciPy, Levenberg−Marquardt algorithm):

$$\left(\frac{\overline{\mathrm{FP}}}{\mathrm{OD}}\right)_{\mathrm{cor}} = f(C) = \mathrm{a} + \mathrm{k}\left(\frac{C^n}{C^n + K_M^n}\right)$$

with C: the concentration of naringenin in the growth medium (mg/L); a: the basal normalized fluorescent signal (leaky expression, au); k: the relative maximum normalized fluorescent signal (au); n: the Hill coefficient (cooperativity, sigmoid character); $K_{M:}$ the Hill constant (half-maximal naringenin concentration, mg/L).

We apply a *Noise* parameter as an indicator for the overall mean error on the response of FdeR. The average relative error was calculated across the imposed naringenin or liquiritigenin concentrations, as follows:

$$\mathrm{Noise} = \sqrt{\sum_{\mathrm{i=0\ mM}}^{1.0\ \mathrm{mM}} \left(\frac{\mathrm{SE_{cor,i}}}{\left(\frac{\overline{\mathrm{FP}}}{\mathrm{OD}}\right)_{\mathrm{cor,i}}}\right)^2}$$

with SE cor,i the standard errors(SE) of the mean values for the imposed naringenin concentrations 0.1, 0.2, 0.3, 0.4, 0.5, 0.6, 0.7, 0.8, 0.9 and 1 mM. We did not take the concentration 0.0 mM naringenin or liquiritigenin and the corresponding response signal into consideration, because they dominate the *Noise* parameter value.

9. Molecular Docking

We used AutoDock 4.2.6[17] for protein-small molecule docking. We obtained the 3D structure of the protein receptor using AlphaFold2 (Figure S10), and then performed a series of operations such as adding hydrogen, merging non-polar hydrogen, assigning Gasteiger charges, and storing it as a PDBQT format file. We obtained the planar conformation of liquiritigenin from PubChem, and then used OpenBabel to perform conformational conversion to form the optimal three-dimensional conformation required for docking and store it as a mol2 format file (Figure S9). Using AutoDockTools (ADT), we performed operations such as adding hydrogen and merging non-polar hydrogen atoms on liquiritigenin, and calculated the Gasteiger-Huiekel charges. The ligand was also stored as a PDBQT format file.

We chose the LGA algorithm for energy optimization, and set the relevant parameters of the Autogrid4 docking box and the Autodock4 docking program, and finally obtained a variety of docking conformations clustered by binding energy and RMSD - the computer selected the docking result with the lowest binding energy, and then used this docking conformation as a reference to compare other docking results. Compared with the control, those with a mean square deviation and structural difference of less than 0.5 Å were grouped into one group (cluster), and those with a difference of more than 0.5 Å were divided into another group. The different docking results in the same group were also sorted by binding energy and compared with the first one in the group. Those with a difference of less than 0.5 Å were left in the group, and those with a difference of more than 0.5 Å were re-grouped, and so on.

We used Discovery Studio to perform DNA 3D modeling of the *fdeR* gene promoter, and then used the protein as the receptor and the promoter as the ligand to perform DNA-protein docking

on pyDockDNA. Then, according to the scoring ranking provided by pyDockDNA, we comprehensively judged and selected the docking results. The final screened conformation was analyzed and plotted using Pymol.

10. Prediction of single mutation sites

We use the software of Discovery Studio 2021 Client to predict the mutation sites. The receptor protein was applied CHARMm force field. Mutation stability was processed on single site using Calculate Mutation Energy (Binding) protocol of Discovery Studio 2021 Client.

Calculate Mutation Energy (Binding) protocol evaluates the effect of single-point mutations on protein stability. It performs amino-acid scanning mutagenesis on a set of selected amino-acid residues by mutating each of them to one or more specified amino-acid types. The mutation energy is the change in the protein's stability caused by a mutation. It is measured by comparing how much energy the protein needs to fold in its original and mutated forms. The more energy the protein needs to fold, the less stable it is.

11. Molecular dynamics (MD) simulations

The molecular dynamics (MD) simulations were carried out by GROMACS 2020.3 software. The amber99sb-ildn force field and the general Amber force field (GAFF) were used to generate the parameter and topology of proteins and ligands, respectively. The simulation box size was optimized with the distance between each atom of the protein and the box greater than 1.0 nm. Then, fill the box with water molecules based on a density of 1. To make the simulation system electrically neutral, the water molecules were replaced with Cl^- and Na^+ ions. Following the steepest descent method, energy optimization of 5.0×10^4 steps was performed to minimize the energy consumption of the entire system, and finally to reduce the unreasonable contact or atom overlap in the entire system. After energy minimization, first-phase equilibration was performed with the NVT ensemble at 300 K for 100 ps to stabilize the temperature of the system. Second-phase equilibration was simulated with the NPT ensemble at 1 bar and 100 ps. The primary objective of the simulation is to optimize the interaction between the target protein and the solvent and ions so that the simulation system is fully pre-equilibrated. All MD simulations were performed for 50 ns under an isothermal and isostatic ensemble with a temperature of 300 K and a pressure of 1 atmosphere. The temperature and pressure were controlled by the V-rescale and Parrinello-Rahman methods, respectively, and the temperature and pressure coupling constants were 0.1 and 0.5 ps, respectively. Lennard-Jones function was used to calculate the Van der Waals force, and the nonbond truncation distance was set to 1.4 nm. The bond length of all atoms was constrained by the LINCS algorithm. The long-range electrostatic interaction was calculated by the Particle Mesh-Ewald method with the Fourier spacing 0.16 nm.

12. DP6 mutation rate assay

DP6 was transformed into S2060 and plated on Chl-resistant 2×YT plates containing 100 mM D-Glucose. Monoclones were picked and shaken till saturation in 2×YT medium containing 25 mM D-Glu and Chl; the above bacterial solution was diluted 103-fold and grown to OD_{600} of 0.5-0.7. Samples were divided into two groups: one with 25 mM D-Glucose and the other with 25

mM arabinose, and incubated for 12h until saturation. Then,the bacterial solution was diluted by gradient and divided into two groups:one was applied to 2×YT plates containing 100 mM D-Glucose and Chl, the other was applied to 2×YT plates containing 100 mM D-Glucose and Rif. Culture them at 37°C for 18-24 h. The number of colonies of each culture on D-Glucose ± Rif plates was counted. Formula for calculating DP6 mutation rate (tbp: substituents per bp per generation): ubp = f/[R × ln(N//N0)], where f is the frequency of rifampin-resistant mutants (as compared with the glucose control), R is the number of unique sites yielding rifampin resistance (Liu *et al.* have identified only 21 sites across both rpoB clusters in their experiments),[29] N is the final population size and N0 is the population size at which resistance is first observed (empirically determined to be B1.5107).

13. Transformation and storage of *E. coli 2060* competent cells and strains prepared by chemical methods

Luciferase assay, phage propagation experiment and PACE were operated in the *E. coli S2060* strain.

Competent cells are prepared by the method below. The saturated S2060 solution was added to a conical flask containing 2 x YT liquid medium (Solarbio) with appropriate antibiotics and diluted 100 times. The flask was then incubated in a shaker at 37℃ at 200-300 rpm/min until the OD_{600} of the bacterial solution was 0.4-0.6. We took and centrifuged 50 mL bacterial solution in the centrifugal tubes t 6500 rpm, 4℃ for 10 min. Discard the supernatant, and add 2 mL cold liquid LB and 2 mL cold 2×TSS ($MgCl_2$, PEG 3350 and DMSO were added to LB medium at final concentrations of 20 mM, 10% and 5% respectively). Then, we froze the competent cells in the liquid nitrogen after mixing and dispensing them in the tubes and stored at -80℃.

As for transformation, 100 μL competent cells defrost on the ice; add pre-cooled plasmid mixture (each kind of plasmids should <100 ng; 3 kinds of plasmids can be transferred at most) and 100 μL 1×KCM (KCl, $CaCl_2$ and $MgCl_2$ were added to LB medium at final concentrations of 100 mM, 30 mM and 50 mM respectively). Put it on the ice for 10 min after being mixedthoroughly, heat shock at 42 ℃ for 75 s; put it on the ice for 2-3 min; add 500 μL SOC solution in it and put it in the biological shaker at 200-300 rpm/min for 1 h; centrifuged the bacterial solution at 8000 rpm for 2 min, discard the supernatant; plate the bacterial solution on the 2×YT solid culture (1.5% agar) with proper antibiotics after the bacterial solution being resuspended; culture at 37 ℃ for 16-18 h. A saturated bacterial solution containing the appropriate antibiotic is mixed in equal proportions with sterile glycerol and stored frozen at -80 ℃.

14. Construction of selection phage

Golden Gate cloning was used to assemble selection phage (SP). For Golden Gate assembly, *Sap* I (New England BioLabs) acted as IIS restriction endonuclease along with T4 DNA ligase (New England BioLabs). Golden Gate cloning reaction mixture was prepared as followes: 3-5 ng/kb/μL donor plasmids and 1-3 ng/kb/μL receptor (pBT137-SplitC and pBT137-SplitD). And the mixtures experienced thermal cycles (37 ℃ for 5 min,16 ℃ for 5 min, 40 cycles, 60 ℃ 5 min, 4 ℃). After this process, assemblies were transferred into S2208 competent cells.

15. Activity-independent phage plaque assay

Saturated S2208 bacterial broth was diluted with 2×YT liquid medium containing Amp and shaken at 37°C to OD_{600} : 0.6-0.9. Phage was diluted 3 times with sterilized water in a gradient of 10^2 . Transfer 10 μL of each different concentration of phage to a centrifuge tube. Add 150 μl of diluted S2208, then 20 μL of X-Gal (dissolve X-Gal in DMF to a final concentration of 2% (wt/vol)) solution, leave for 5 min, add 1mL of hot 2×YT top agar, mix well and pour the above mixture onto 2×YT solid agar tetrads at 37 °C for 5-8 h. Calculate the phage titer: Phage titer number of phage spots in the corresponding quadrant × dilution × 100.

16. Isolation of colonies

Gently touch the plaque with the tip of a P10 pipette. Place the pipette tip into 2-3 mL of DRM, grow for 16-20 h in a biological shaker at 37℃. Centrifuge at 8000 g for 2 min. The supernatant was collected and filtered in a 1 ml syringe equipped with a PVDF filter (13 mm 0.22 μm) to obtain a phage stock solution. Its concentration was determined using an activity-independent phage plaque assay. POI fragments can also be amplified by PCR for sequencing.

17. Activity-dependent plaque test

S2060 saturated bacterial solution transformed with AP was diluted 1000 times into DRM medium containing appropriate antibiotics, and the culture was shaken at 37 ℃ until OD_{600} grow to 0.4-0.6. Cells were infected with phage at a starting titer of approximately 10^4 PFU/ml and incubated at 37 ℃ for 16-20 h on a biological shaker. Centrifuge at 8000 g for 3 min. The supernatant was collected and filtered in a 1ml syringe equipped with a PVDF filter (13 mm 0.22 μm) to obtain phage stock solution, which was stored at -4 ℃.

18. Purification of SP

In the above transformation step, the above plasmids were replaced with a mixture product of assembled SP plasmids, heat shocked for 75 s, left on ice for 2-3 min, and then the cell mixture was directly diluted into 10ml of antibiotic-free 2×YT liquid medium at 37 ℃ for 16-18 h at 200-300 rpm/min on a biologicalshaker. 2 mL of bacterial solution was put into a centrifuge tube and centrifuged at 8000 g for 3 min. The supernatant was collected and filtered in a 1 ml syringe (Nanjing Dingbei Biotechnology co., LTD.) equipped with a PVDF filter (13 mm 0.22 μm) (Nanjing Dingbei Biotechnology co., LTD.) to obtain the phage stock solution and stored at -4℃.

References:

1. M. Ramalingam, H. Kim Y. Lee *et al*, Phytochemical and Pharmacological Role of Liquiritigenin and Isoliquiritigenin From Radix Glycyrrhizae in Human Health and Disease Models. *Front Aging Neurosci* **10**, 348, (2018).
   DOI: http://doi.org/10.3389/fnagi.2018.00348
2. J.A. Chemler, Y. Yan M.A. Koffas, Biosynthesis of isoprenoids, polyunsaturated fatty acids and flavonoids in Saccharomyces cerevisiae. *Microb Cell Fact* **5**, 20, (2006).
   DOI: http://doi.org/10.1186/1475-2859-5-20
3. Y. Katsuyama, M. Matsuzawa N. Funa *et al*, Production of curcuminoids by Escherichia coli

carrying an artificial biosynthesis pathway. *Microbiology (Reading)* **154**, 2620-2628, (2008). DOI: http://doi.org/10.1099/mic.0.2008/018721-0

4. J. Li, F. Xu D. Ji *et al*, Diversion of metabolic flux towards 5-deoxy(iso)flavonoid production via enzyme self-assembly in Escherichia coli. *Metabolic Engineering Communications* **13**, e00185, (2021). DOI: http://doi.org/https://doi.org/10.1016/j.mec.2021.e00185
5. S.G. Stahlhut, S. Siedler S. Malla *et al*, Assembly of a novel biosynthetic pathway for production of the plant flavonoid fisetin in Escherichia coli. *Metabolic engineering* **31**, 84-93, (2015). DOI: https://doi.org/10.1016/j.ymben.2015.07.002.
6. S. Jang, S. Jang Y. Xiu *et al*, Development of Artificial Riboswitches for Monitoring of Naringenin In Vivo. *ACS Synth Biol* **6**, 2077-2085, (2017). DOI: http://doi.org/10.1021/acssynbio.7b00128
7. A.M. Marin, E.M. Souza F.O. Pedrosa *et al*, Naringenin degradation by the endophytic diazotroph Herbaspirillum seropedicae SmR1. *Microbiology (Reading)* **159**, 167-175, (2013). DOI: http://doi.org/10.1099/mic.0.061135-0
8. M.S. Packer, H.A. Rees D.R. Liu, Phage-assisted continuous evolution of proteases with altered substrate specificity. *Nat Commun* **8**, 956, (2017). DOI: http://doi.org/10.1038/s41467-017-01055-9
9. S.V. Harbaugh, A.D. Silverman Y.G. Chushak *et al*, Engineering a Synthetic Dopamine-Responsive Riboswitch for In Vitro Biosensing. *ACS Synth Biol* **11**, 2275-2283, (2022). DOI: http://doi.org/10.1021/acssynbio.1c00560
10. C.A. Kellenberger, S.C. Wilson S.F. Hickey *et al*, GEMM-I riboswitches from Geobacter sense the bacterial second messenger cyclic AMP-GMP. *Proc Natl Acad Sci U S A* **112**, 5383-8, (2015). DOI: http://doi.org/10.1073/pnas.1419328112
11. D. Bose, Y. Su A. Marcus *et al*, An RNA-Based Fluorescent Biosensor for High-Throughput Analysis of the cGAS-cGAMP-STING Pathway. *Cell Chem Biol* **23**, 1539-1549, (2016). DOI: http://doi.org/10.1016/j.chembiol.2016.10.014
12. X.C. Wang, S.C. Wilson M.C. Hammond, Next-generation RNA-based fluorescent biosensors enable anaerobic detection of cyclic di-GMP. *Nucleic Acids Res* **44**, e139, (2016). DOI: http://doi.org/10.1093/nar/gkw580
13. S. Siedler, S.G. Stahlhut S. Malla *et al*, Novel biosensors based on flavonoid-responsive transcriptional regulators introduced into Escherichia coli. *Metab Eng* **21**, 2-8, (2014). DOI: http://doi.org/10.1016/j.ymben.2013.10.011
14. B. De Paepe, J. Maertens B. Vanholme *et al*, Modularization and Response Curve Engineering of a Naringenin-Responsive Transcriptional Biosensor. *ACS Synth Biol* **7**, 1303-1314, (2018). DOI: http://doi.org/10.1021/acssynbio.7b00419
15. J. Vandierendonck, Y. Girardin P. De Bruyn *et al*, A Multi-Layer-Controlled Strategy for Cloning and Expression of Toxin Genes in Escherichia coli. *Toxins (Basel)* **15**, (2023). DOI: http://doi.org/10.3390/toxins15080508
16. J. Jumper, R. Evans A. Pritzel *et al*, Highly accurate protein structure prediction with AlphaFold. *Nature* **596**, 583-589, (2021). DOI: http://doi.org/10.1038/s41586-021-03819-2
17. G.M. Morris, R. Huey W. Lindstrom *et al*, AutoDock4 and AutoDockTools4: Automated docking

with selective receptor flexibility. *J Comput Chem* **30**, 2785-91, (2009).
DOI: http://doi.org/10.1002/jcc.21256

18. BIOVIA, Dassault Systèmes, Discovery Studio Visualizer, v21.1.0.20298, San Diego: Dassault Systèmes, 2020.
19. R. Wassem, A.M. Marin A. Daddaoua *et al*, A NodD-like protein activates transcription of genes involved with naringenin degradation in a flavonoid-dependent manner in Herbaspirillum seropedicae. *Environ Microbiol* **19**, 1030-1040, (2017).
DOI: http://doi.org/10.1111/1462-2920.13604
20. Y. Jiang, J. Gu J. Lei *et al*, Molecular Dynamics and Bioactivity of a Novel Mutated Human Parathyroid Hormone. *Tropical Journal of Pharmaceutical Research* **13**, 511-518, (2014).
DOI:http://doi.org/10.4314/tjpr.v13i4.4
21. K.L. MacQuarrie, A.P. Fong R.H. Morse *et al*, Genome-wide transcription factor binding: beyond direct target regulation. *Trends Genet* **27**, 141-8, (2011).
DOI: http://doi.org/10.1016/j.tig.2011.01.001
22. K.M. Esvelt, J.C. Carlson D.R. Liu, A system for the continuous directed evolution of biomolecules. *Nature* **472**, 499-503, (2011).
DOI: http://doi.org/10.1038/nature09929
23. A.H. Badran, V.M. Guzov Q. Huai *et al*, Continuous evolution of Bacillus thuringiensis toxins overcomes insect resistance. *Nature* **533**, 58-63, (2016).
DOI: http://doi.org/10.1038/nature17938
24. D.I. Bryson, C. Fan L.T. Guo *et al*, Continuous directed evolution of aminoacyl-tRNA synthetases. *Nat Chem Biol* **13**, 1253-1260, (2017).
DOI: http://doi.org/10.1038/nchembio.2474
25. A.H. Badran D.R. Liu, Development of potent in vivo mutagenesis plasmids with broad mutational spectra. *Nat Commun* **6**, 8425, (2015).
DOI: http://doi.org/10.1038/ncomms9425
26. J.C. Carlson, A.H. Badran D.A. Guggiana-Nilo *et al*, Negative selection and stringency modulation in phage-assisted continuous evolution. *Nat Chem Biol* **10**, 216-22, (2014).
DOI: http://doi.org/10.1038/nchembio.1453
27. T.P. Huang, Z.J. Heins S.M. Miller *et al*, High-throughput continuous evolution of compact Cas9 variants targeting single-nucleotide-pyrimidine PAMs. *Nat Biotechnol* **41**, 96-107, (2023).
DOI: http://doi.org/10.1038/s41587-022-01410-2
28. T. Wei, W. Lai Q. Chen *et al*, Exploiting spatial dimensions to enable parallelized continuous directed evolution. *Mol Syst Biol* **18**, e10934, (2022).
DOI: http://doi.org/10.15252/msb.202210934
29. P. Carbonell, T. Radivojevic M.H. Garcia, Opportunities at the Intersection of Synthetic Biology, Machine Learning, and Automation. *ACS Synth Biol* **8**, 1474-1477, (2019).
DOI: http://doi.org/10.1021/acssynbio.8b00540
30. B.P. Hubbard, A.H. Badran J.A. Zuris *et al*, Continuous directed evolution of DNA-binding proteins to improve TALEN specificity. *Nat Methods* **12**, 939-42, (2015).
DOI: http://doi.org/10.1038/nmeth.3515
31. S.M. Miller, T. Wang P.B. Randolph *et al*, Continuous evolution of SpCas9 variants compatible with non-G PAMs. *Nat Biotechnol* **38**, 471-481, (2020).
DOI: http://doi.org/10.1038/s41587-020-0412-8

Acknowledgments

We are grateful to the support of Nanjing Agricultural University (NAU). We sincerely thank professor Xi Chen and professor Xin Yan for providing materials and their advice.

Author contributions

Z.M.L conceived and designed the project with conceptual and practical guidance from C.X. and Y.X., H.T.Q., L.Y., L.Y.X., Y.Y.X., Z.M.L. performed experiments with support from L.J., L.J.J. and N.X.H.; Y.Y.H., Z.Y. and Z.Y.H. wrote the article with contributions from other authors; F.S.W. and C.K.X. provided some figures in the article; S.H.Z. accounted for the computational experiments. C.X. and Y.X. agree to serve as corresponding authors and ensures communication.

Competing interests

The authors declare no competing interests.

Supplementary information is available for this paper in the online version.